The first returned samples from a C-type asteroid show kinship to the chemically most primitive meteorites

Tetsuya Yokoyama[1]†, Kazuhide Nagashima[2]†, Izumi Nakai[3], Edward D. Young[4], Yoshinari Abe[5], Jérôme Aléon[6], Conel M. O'D. Alexander[7], Sachiko Amari[8], Yuri Amelin[9], Ken-ichi Bajo[10], Martin Bizzarro[11], Audrey Bouvier[12], Richard W. Carlson[7], Marc Chaussidon[13], Byeon-Gak Choi[14], Nicolas Dauphas[15], Andrew M. Davis[15], Tommaso Di Rocco[16], Wataru Fujiya[17], Ryota Fukai[18], Ikshu Gautam[1], Makiko K. Haba[1], Yuki Hibiya[19], Hiroshi Hidaka[20], Hisashi Homma[21], Peter Hoppe[22], Gary R. Huss[2], Kiyohiro Ichida[23], Tsuyoshi Iizuka[24], Trevor R. Ireland[25], Akira Ishikawa[1], Motoo Ito[26], Shoichi Itoh[27], Noriyuki Kawasaki[10], Noriko T. Kita[28], Kouki Kitajima[28], Thorsten Kleine[29], Shintaro Komatani[23], Alexander N. Krot[2], Ming-Chang Liu[4], Yuki Masuda[1], Kevin D. McKeegan[4], Mayu Morita[23], Kazuko Motomura[30], Frédéric Moynier[13], Ann Nguyen[31], Larry Nittler[7], Morihiko Onose[23], Andreas Pack[16], Changkun Park[32], Laurette Piani[33], Liping Qin[34], Sara S. Russell[35], Naoya Sakamoto[36], Maria Schönbächler[37], Lauren Tafla[4], Haolan Tang[4], Kentaro Terada[38], Yasuko Terada[39], Tomohiro Usui[18], Sohei Wada[10], Meenakshi Wadhwa[40], Richard J. Walker[41], Katsuyuki Yamashita[42], Qing-Zhu Yin[43], Shigekazu Yoneda[44], Hiroharu Yui[45], Ai-Cheng Zhang[46], Harold C. Connolly, Jr.[47], Dante S. Lauretta[48], Tomoki Nakamura[49], Hiroshi Naraoka[50], Takaaki Noguchi[27], Ryuji Okazaki[50], Kanako Sakamoto[18], Hikaru Yabuta[51], Masanao Abe[18], Masahiko Arakawa[52], Atsushi Fujii[18], Masahiko Hayakawa[18], Naoyuki Hirata[52], Naru Hirata[53], Rie Honda[54], Chikatoshi Honda[53], Satoshi Hosoda[18], Yu-ichi Iijima[18]‡, Hitoshi Ikeda[18], Masateru Ishiguro[14], Yoshiaki Ishihara[18], Takahiro Iwata[18,64], Kosuke Kawahara[18], Shota Kikuchi[55], Kohei Kitazato[53], Koji Matsumoto[56], Moe Matsuoka[18]§, Tatsuhiro Michikami[57], Yuya Mimasu[18], Akira Miura[18], Tomokatsu Morota[58], Satoru Nakazawa[18], Noriyuki Namiki[56], Hirotomo Noda[56], Rina Noguchi[59], Naoko Ogawa[18], Kazunori Ogawa[18], Tatsuaki Okada[18], Chisato Okamoto[52]‡, Go Ono[18], Masanobu Ozaki[18,64], Takanao Saiki[18], Naoya Sakatani[60], Hirotaka Sawada[18], Hiroki Senshu[55], Yuri Shimaki[18], Kei Shirai[18], Seiji Sugita[58], Yuto Takei[18], Hiroshi Takeuchi[18], Satoshi Tanaka[18], Eri Tatsumi[61], Fuyuto Terui[62], Yuichi Tsuda[18], Ryudo Tsukizaki[18], Koji Wada[55], Sei-ichiro Watanabe[20], Manabu Yamada[55], Tetsuya Yamada[18], Yukio Yamamoto[18], Hajime Yano[18], Yasuhiro Yokota[18], Keisuke Yoshihara[18], Makoto Yoshikawa[18], Kent Yoshikawa[18], Shizuho Furuya[18], Kentaro Hatakeda[18], Tasuku Hayashi[18], Yuya Hitomi[18], Kazuya Kumagai[18], Akiko Miyazaki[18], Aiko Nakato[18], Masahiro Nishimura[18], Hiromichi Soejima[18], Ayako Suzuki[18], Toru Yada[18], Daiki Yamamoto[18], Kasumi Yogata[18], Miwa Yoshitake[18], Shogo Tachibana[63], Hisayoshi Yurimoto[10]*

Affiliations:

[1]Department of Earth and Planetary Sciences, Tokyo Institute of Technology; Tokyo 152-8551, Japan.

[2]Hawai'i Institute of Geophysics and Planetology, University of Hawai'i at Mānoa; Honolulu, HI 96822, USA.

[3]Applied Chemistry, Tokyo University of Science; Tokyo 162-8601, Japan.

[4]Earth, Planetary, and Space Sciences, UCLA; Los Angeles, CA 90095, USA.

[5]Graduate School of Engineering Materials Science and Engineering, Tokyo Denki University; Tokyo 120-8551, Japan.

[6] Institut de Minéralogie, de Physique des Matériaux et de Cosmochimie, Sorbonne Université, Museum National d'Histoire Naturelle, CNRS UMR 7590, IRD; 75005 Paris, France.

[7] Earth and Planets Laboratory, Carnegie Institution for Science; Washington, DC, 20015, USA.

[8] McDonnell Center for the Space Sciences and Physics Department, Washington University; St. Louis, MO 63130, USA.

[9] Guangzhou Institute of Geochemistry, Chinese Academy of Sciences; Guangzhou, GD 510640, China.

[10] Natural History Sciences, IIL, Hokkaido University; Sapporo 001-0021, Japan.

[11] Centre for Star and Planet Formation, GLOBE Institute, University of Copenhagen; Copenhagen, K 1350, Denmark.

[12] Bayerisches Geoinstitut, Universität Bayreuth; Bayreuth 95447, Germany.

[13] Université de Paris, Institut de physique du globe de Paris, CNRS; 75005 Paris, France

[14] Department of Physics and Astronomy, Seoul National University; Seoul 08826, Republic of Korea.

[15] Department of the Geophysical Sciences and Enrico Fermi Institute, The University of Chicago; Chicago, IL 60637, USA.

[16] Faculty of Geosciences and Geography, University of Göttingen; Göttingen, D-37077, Germany.

[17] Faculty of Science, Ibaraki University; Mito 310-8512, Japan.

[18] ISAS/JSEC, JAXA; Sagamihara 252-5210, Japan.

[19] General Systems Studies, The University of Tokyo; Tokyo 153-0041, Japan.

[20] Earth and Planetary Sciences, Nagoya University; Nagoya 464-8601, Japan.

[21] Osaka Application Laboratory, SBUWDX, Rigaku Corporation; Osaka 569-1146, Japan.

[22] Max Planck Institute for Chemistry; Mainz 55128, Germany.

[23] Analytical Technology, Horiba Techno Service Co., Ltd.; Kyoto 601-8125, Japan.

[24] Earth and Planetary Science, The University of Tokyo; Tokyo 113-0033, Japan.

[25] School of Earth and Environmental Sciences, The University of Queensland; St Lucia QLD 4072, Australia.

[26] Kochi Institute for Core Sample Research, JAMSTEC; Kochi 783-8502, Japan.

[27] Earth and Planetary Sciences, Kyoto University; Kyoto 606-8502, Japan.

[28] Geoscience, University of Wisconsin- Madison; Madison, WI 53706, USA.

[29] Max Planck Institute for Solar System Research; 37077 Göttingen, Germany.

[30] Thermal Analysis, Rigaku Corporation; Tokyo 196-8666, Japan.

[31] Astromaterials Research and Exploration Science, NASA Johnson Space Center; Houston, TX 77058, USA.

[32]Earth-System Sciences, Korea Polar Research Institute; Incheon 21990, Korea.

[33]Centre de Recherches Pétrographiques et Géochimiques, CNRS - Université de Lorraine; 54500 Nancy, France.

[34]University of Science and Technology of China, School of Earth and Space Sciences; Anhui 230026, China.

[35]Department of Earth Sciences, Natural History Museum; London, SW7 5BD, UK.

[36]IIL, Hokkaido University; Sapporo 001-0021, Japan.

[37]Institute for Geochemistry and Petrology, Department of Earth Sciences, ETH Zurich, Zurich, Switzerland.

[38]Earth and Space Science, Osaka University; Osaka 560-0043, Japan.

[39]Spectroscopy and Imaging, Japan Synchrotron Radiation Research Institute; Hyogo 679-5198 Japan.

[40]School of Earth and Space Exploration, Arizona State University; Tempe, AZ 85281, USA.

[41]Geology, University of Maryland, College Park, MD 20742, USA.

[42]Graduate School of Natural Science and Technology, Okayama University; Okayama 700-8530, Japan.

[43]Earth and Planetary Sciences, University of California; Davis, CA 95616, USA.

[44]Science and Engineering, National Museum of Nature and Science; Tsukuba 305-0005, Japan.

[45]Chemistry, Tokyo University of Science; Tokyo 162-8601, Japan.

[46]School of Earth Sciences and Engineering, Nanjing University; Nanjing 210023, China.

[47]Department of Geology, School of Earth and Environment, Rowan University; Glassboro, NJ 08028, USA.

[48]Lunar and Planetary Laboratory, University of Arizona; Tucson, AZ 85705, USA.

[49]Department of Earth Science, Tohoku University; Sendai, 980-8578, Japan.

[50]Department of Earth and Planetary Sciences, Kyushu University; Fukuoka 819-0395, Japan.

[51]Earth and Planetary Systems Science Program, Hiroshima University; Higashi-Hiroshima, 739-8526, Japan.

[52]Kobe University; Kobe 657-8501, Japan.

[53]University of Aizu; Aizu-Wakamatsu 965-8580, Japan.

[54]Kochi University; Kochi 780-8520, Japan.

[55]Chiba Institute of Technology; Narashino 275-0016, Japan.

[56]National Astronomical Observatory of Japan; Mitaka 181-8588, Japan.

[57]Kinki University; Higashi-Hiroshima 739-2116, Japan.

[58]The University of Tokyo; Tokyo 113-0033, Japan.

[59]Niigata University; Niigata 950-2181, Japan.

[60]Rikkyo University; Tokyo 171-8501, Japan.

[61]Instituto de Astrofísica de Canarias, University of La Laguna; Tenerife, Spain.

[62]Kanagawa Institute of Technology; Atsugi 243-0292, Japan.

[63]UTokyo Organization for Planetary and Space Science, University of Tokyo; Tokyo 113-0033, Japan.

[64]The Graduate University for Advanced Studies, SOKENDAI, Kanagawa 240-0193, Japan

*Corresponding author. Email: yuri@ep.sci.hokudai.ac.jp

†These authors contributed equally to this work.

‡Deceased.

§Present address. LESIA, Observatoire de Paris; 92195 Meudon, France.

Abstract:

Bulk chemical and isotopic compositions, and mineralogy in the asteroid (162173) Ryugu samples show that Ryugu is mainly composed of materials related to the CI (Ivuna-like) carbonaceous chondrite group. The samples consist predominantly of minerals produced by aqueous alteration in a parent planetesimal from which Ryugu was derived. The ^{53}Mn-^{53}Cr systematics of dolomite suggest that this alteration occurred 5.2 (+0.7/–0.8) million years after formation of Ca-Al-rich inclusions, the first solids formed in the Solar System. The aqueous alteration temperature at the time dolomite and magnetite coprecipitated was 37±10°C. Unlike in CI chondrites, phyllosilicates in Ryugu have lost most of their interlayer water, but retained structural water. This indicates that following aqueous alteration the Ryugu samples avoided heating above ~90°C.

(120 words; 100-125 words)

One-Sentence Summary:

Returned samples from C-type asteroid Ryugu show strong similarities to CI (Ivuna-like) carbonaceous chondrites.

(112 characters; <125 characters and spaces)

Main Text:

Although it is generally accepted that meteorites are fragments of asteroids, specific meteorite-asteroid connections are poorly understood. Samples of asteroid (25143) Itokawa returned by the JAXA Hayabusa mission revealed that S-type asteroids are composed of materials consistent with the ordinary chondrite class (*1, 2*). The JAXA Hayabusa2 (*3*) spacecraft was launched on December 3rd, 2014 to rendezvous with and sample the near-Earth Cb-type asteroid (162173) Ryugu with the aim of clarifying the relationship between C-type asteroids and the carbonaceous chondrite class. Remote sensing observations of Ryugu from Hayabusa2 revealed that: (*i*) Ryugu's albedo is darker than that of every known meteorite group (*4, 5*); (*ii*) Ryugu contains ubiquitous phyllosilicates, as shown by an absorption band at 2.72 μm (*4, 6*); (*iii*) the strength and shape of this absorption band as compared to those from laboratory heating experiments of carbonaceous chondrites suggests that Ryugu's surface experienced heating above 300 °C (*6*); and (*iv*) Ryugu materials are probably more porous than any known carbonaceous chondrite, as shown by measurements of the thermal inertia (*7, 8*). These results indicated that carbonaceous-chondrite-class materials are plausible constituents of Ryugu, but no known carbonaceous chondrite completely matches the Ryugu remote-sensing observations. Laboratory examination of the fragments returned by Hayabusa2 paints a much sharper picture of the constituents and history of Ryugu.

The Hayabusa2 spacecraft made two successful landings onto Ryugu to collect asteroidal materials in 2019 (*9*) and delivered the collected samples to Earth on December 6th, 2020. The returned samples are detritus ranging in size from <10 μm to ~10 mm, with a total mass exceeding 5 grams. Their colors, shapes, and macro-structures are consistent with those acquired by remote sensing observations, indicating that the returned samples are representative of the asteroid Ryugu (*10, 11*). The returned samples were recovered in a non-destructive manner and the initial description was performed under strict contamination-controlled conditions at the JAXA Extraterrestrial Sample Curation Center prior to delivery to the Initial Analysis teams (*10*). The initial analysis of the Ryugu samples began in June 2021. At that time, ~125 mg of samples, containing both powder and particles from the first and the second touchdown sites, were allocated to the Initial Analysis Chemistry Team.

The goals of the Initial Analysis Chemistry Team investigations are to provide fundamental answers to questions related to the provenance of Ryugu samples. It is also to provide the framework for future in-depth research by the international scientific community. In particular, the team aimed to address the following questions: (*i*) what are the bulk elemental abundances of Ryugu; (*ii*) what are the bulk isotopic compositions of Ryugu; (*iii*) does Ryugu consist of primary materials formed in the protosolar disk or of secondary materials formed in Ryugu or a precursor asteroid; (*iv*) when were Ryugu's constituent materials formed; and (*v*) what, if any, relationship does Ryugu have with known meteoritic samples?

In this paper, we report the chemical and isotopic characteristics of the Ryugu samples and outline the general history of Ryugu from accretion to present. We also discuss the implications of our results have for the origin of the CI chondrite group and, more generally, for cosmochemistry.

Petrology and mineralogy

The Ryugu samples are mixtures of brecciated fine-grained matrix materials composed of phyllosilicates, predominantly serpentine and saponite, and coarser grains dominated by carbonates, magnetite, and sulfides (Fig. 1) (*12*). Neither Ca-Al-rich inclusions (CAIs) nor

chondrules, which are characteristic of most chondrites, nor their relicts, were evident in the allocated samples. The serpentine/saponite molar ratio is approximately 6/4, based on the bulk chemical composition of the matrix. The coarser-grained minerals in the Ryugu polished section studied here are dolomite ($CaMg(CO_3)_2$), breunnerite ((Mg, Fe, $Mn)CO_3$), pyrrhotite ($Fe_{1-x}S$), and magnetite (Fe_3O_4); they are distributed throughout the matrix, as well as in the veinlets. Calcite ($CaCO_3$), pentlandite (($Fe,Ni)_9S_8$), cubanite ($CuFe_2S_3$), ilmenite ($FeTiO_3$), apatite (($Ca_5(PO_4)_3(OH,F,Cl)$)), and Mg-Na-phosphate are accessory minerals. Anhydrous silicates such as olivine and pyroxene, which are common in chondrites, are very rare and occur as discrete grains smaller than ~10 μm across. Overall, the petrology and mineralogy of the Ryugu samples resemble the extensively aqueously altered CI chondrites (*13*). However, sulfates and ferrihydrite, which are commonly observed in CI chondrites, were not identified in the samples studied. The mineral assemblages of the Ryugu samples observed here are generally consistent with the results of (*14*); it is noted that small altered chondrules and CAIs were identified in the samples in that study.

Bulk chemical and isotopic compositions

No systematic differences in chemical composition are observed between samples from the first and the second touchdown sites (Fig. 2) (*12*). The observed variations in bulk composition are most likely due to heterogeneity at the small scales sampled and analyzed, as the masses of the samples analyzed were less than 30 mg and coarser-grained water-precipitated minerals may not be uniformly distributed at that scale (Fig. 1). Clear spatial heterogeneity in the mineral distributions is observed for carbonates (dolomite) and sulfides (pyrrhotite), both of which precipitated from aqueous solution during alteration of the protolith (Fig. 1). There is, for example, a difference in the concentrations of the rare earth elements (REEs) between the fragments A0106-A0107 from the first touchdown site and C0108 from the second touchdown site (*12*), which are both elevated relative to CI chondrites (Fig. 2). These variable enrichments could be explained by depletion of H_2O, relative to CI chondrites (see next paragraph), and the heterogeneous distribution of REE-rich Ca-phosphate grains (*15, 16*). Such heterogeneity at similar scales has been observed in CI chondrites (*17, 18*) and in the ungrouped carbonaceous chondrite Tagish Lake (*19*).

We do not observe systematic depletions of elemental abundances, relative to CI chondrites, as a function of volatility. In contrast, other groups of carbonaceous chondrites show various degrees of depletion in volatile elements (*20*). The lack of systematic depletion in the moderately and highly volatile elements of the Ryugu fragments strongly supports the view that Ryugu is composed of materials that are related to the CI chondrite group. However, the elemental abundances of hydrogen and oxygen are strikingly depleted in the Ryugu samples compared to CI chondrites, suggesting depletion in H_2O.

Previous studies have revealed a dichotomy in the isotopic composition of titanium and chromium between non-carbonaceous (NC) and carbonaceous (CC) meteorites (*21, 22, 23*). The bulk titanium and chromium isotopic compositions of the Ryugu samples plot close to the CB (Bencubbin-like) and CI chondrite values in the CC meteorite region (Fig. 3). However, the metal-rich nature of CB chondrites likely precludes their kinship with the Ryugu samples.

Oxygen isotopic composition

The whole-rock oxygen isotopic compositions of bulk Ryugu samples are distributed parallel to the terrestrial fractionation line over a range that overlaps with those of the bulk Orgueil CI chondrite samples (Fig. 4) (*12*). The variation in $\delta^{18}O$ is thought to be due to the

heterogeneous distributions of the constituent minerals with very different isotopic compositions, including phyllosilicates, carbonates, and magnetite. On the other hand, two roughly 2-mg-sized Ryugu samples analyzed at the University of California, Los Angeles (UCLA) have $\Delta^{17}O$ values (permil deviation from the terrestrial fractionation line) (*12*) that are identical within the uncertainties, giving an average $\Delta^{17}O = 0.68 \pm 0.05$ ‰ (2 standard deviations (SD)). The sample analyzed at University of Göttingen (UG) is slightly different with $\Delta^{17}O = 0.44 \pm 0.05$ ‰. The two Ryugu samples analyzed at UCLA have higher $\Delta^{17}O$ values than those for the three Orgueil chondrite samples ($\Delta^{17}O = 0.42 – 0.53$ ‰) analyzed in the same analytical session. The range in Orgueil values obtained at UG is similar ($\Delta^{17}O = 0.39 – 0.57$ ‰), suggesting that the differences between the Ryugu samples analyzed in the two laboratories are likely attributable to heterogeneity among the Ryugu samples at the mg scale. Nonetheless, the average $\Delta^{17}O$ value of the three Ryugu samples, 0.61 ± 0.08 (2SD), is somewhat higher than the average for the Orgueil samples in this study of 0.50 ± 0.04 (2SD, $n=5$), a single measurement of the Ivuna CI chondrite samples of 0.41 ± 0.05 ‰, and prior measurements of CI chondrites ($0.39 – 0.47$ ‰, (*24*)), which are all broadly comparable to each other. The difference may reflect either primary heterogeneity between mg-sized samples, or is the result of minor contamination of the meteorite samples by terrestrial water in the phyllosilicates, sulfates, and iron oxides/hydroxides. We note that the discrepancy in the $\Delta^{17}O$ values between Ryugu and Orgueil at UCLA (~–0.15 ‰ for Orgueil) persists despite heating both groups of samples to ~116 °C for 2–4 hours to remove adsorbed water, suggesting that the terrestrial contamination in the Orgueil samples, if present, is part of the structure of the minerals and not simply adsorbed to surfaces.

Dolomite grains in the studied Ryugu samples are enriched in ^{18}O relative to the whole rock values but have the same $\Delta^{17}O$ values within measurement uncertainty, indicating that the constituent minerals generally lie along a single mass fractionation line within their uncertainties (Fig. 4) (*12*). The oxygen isotopic compositions of dolomite in Ryugu overlap with those of dolomite from Ivuna in the three-isotope oxygen diagram. Ryugu magnetite is depleted in ^{18}O relative to the whole rock value and also plots on the Ryugu mass fractionation line with the exception of one measurement that clearly lies above it. The range of Ryugu magnetite grains in the three-isotope oxygen diagram is consistent with that of Ivuna (*25, 26*). The distributions of $^{18}O/^{16}O$ ratios and the relative consistency of $\Delta^{17}O$ values are indicative of isotopic equilibrium during growth of the secondary minerals produced by aqueous alteration. Nevertheless, oxygen isotopic equilibrium between dolomite and magnetite should be strictly evaluated only in microscale regions.

The dolomite grain #1 and magnetite grains #1, 3, 4, and 8 are located within ~100 μm of one another in the A0058-C1001 section (Fig. S1). The dolomite $\Delta^{17}O$ value is –0.7 ±0.9 ‰ (2SD) (*12*). The magnetite grains have the same oxygen isotopic compositions within their uncertainties with a mean $\Delta^{17}O$ value of –0.1 ±0.4 ‰ (2 standard error (SE)). Since the $\Delta^{17}O$ values of dolomite and magnetite grains overlap within error, they appear to have precipitated from the same fluid. Assuming equilibrium, we can use oxygen-isotope thermometry (*27-30*) to estimate the temperature at which the dolomite-magnetite pair precipitated. The $\delta^{18}O$ values of the dolomite and magnetite are 29.9 ±0.9 (2SD) ‰ and –3.0 ±1.1 (2SD) ‰, respectively. The difference in $\delta^{18}O$ values between the dolomite and magnetite is 32.9 ±1.4 ‰, corresponding to an equilibration temperature of 37 ±10 °C (Fig. S2). The temperature is in the range (10 – 150 °C) of previous estimates for aqueous alteration of CI chondrites (*19, 24, 31-37*).

The oxygen isotopic compositions of the water and serpentine that would have been in equilibrium with magnetite and dolomite are calculated to be ($\delta^{18}O$, $\delta^{17}O$) = (1.0 ±1.0 ‰, 0.3

±1.0 ‰) and (18.6 ±2.0 ‰, 9.2 ±1.0 ‰), respectively (Fig. S2). The inferred oxygen isotopic composition of the serpentine is similar to that of the whole rock value within the uncertainties, as expected based on the high abundance of serpentine in the samples. The overall consistency between the estimated equilibration temperatures and the previous work that also indicated relatively low temperatures during CI alteration suggests that oxygen-isotope equilibrium was achieved, or at least nearly so, in the Ryugu samples during aqueous alteration.

^{53}Mn-^{53}Cr isotope systematics

The timing of dolomite and magnetite precipitation during aqueous alteration can be determined with the ^{53}Mn-^{53}Cr system (*12*), based on the decay of the short-lived radionuclide ^{53}Mn to ^{53}Cr ($t_{1/2}$ =3.7 Myr). Manganese-chromium isochrons for dolomite in the Ryugu and Ivuna samples are shown in Figure 5. The initial ^{53}Mn/^{55}Mn ratios obtained from these isochrons are (2.55 ±0.35) ×10^{-6} for Ryugu and (3.14 ±0.28) ×10^{-6} for Ivuna. These initial values are consistent with those of CI dolomites obtained in previous studies (*38, 39*). If we use the initial ^{53}Mn/^{55}Mn ratio of the D'Orbigny angrite (*40*) and U-corrected Pb-Pb ages of D'Orbigny and CV CAIs (*41-43*), the initial ^{53}Mn/^{55}Mn ratio for the Ryugu sample suggests that dolomite precipitation occurred at 5.2 (+0.8/-0.7) million years after CAI formation, which is taken to represent the birth of the Solar System. However, the dolomite precipitation age includes some uncertainty because the initial Solar System ratio of ^{53}Mn/^{55}Mn has not been defined precisely. The dolomite precipitation age changes to 4.8 million years and 6.8 million years after the birth of the Solar System if we use the Solar System initial ^{53}Mn/^{55}Mn ratios proposed by (*44*) and (*45*), respectively. We note that there may be a small systematic uncertainty in the ^{53}Mn-^{53}Cr age due to the inherent analytical limitations of SIMS (*12*).

Speciation of H_2O and CO_2 sources

The mass loss and differential thermogravimetric (DTG) curves (*12*) of our Ivuna sample (Fig. 6) are similar to those reported by (*46*). On the other hand, the total mass loss (15.38 wt.%) of the Ryugu sample is significantly smaller than that of Ivuna (Data S6). The species responsible for the mass loss are mainly H_2O, CO_2 and SO_2 for both Ivuna and Ryugu, although the SO_2 was not quantified for lack of an appropriate standard (Fig. 6).

The total weights calculated by H_2O and CO_2 gases released from the Ryugu sample measured by mass spectrometry coupled with thermogravimetric analysis (TG-MS) (20.78 wt.%) are larger than the real total mass loss (15.38 wt.%) measured by TG (*12*), indicating that carbonates were not the only sources of CO_2 during the TG-MS measurement, but organic carbon was oxidized to CO_2 by residual O_2 in the He flow. This oxidation caused the excess CO_2 measured by the mass spectrometry. Because decomposition of carbonates occurs within a small temperature range (*46*), the sharp CO_2 peaks at 600–800 °C (Fig. 6) can be confidently attributed to carbonates. There were double peaks for Ryugu carbonates. Ryugu samples contain three carbonates (dolomite, breunnerite, and calcite). We could not attribute the peak to specific carbonates because of the limited Ryugu samples allocated for this work. The double peaks might be due to sealed pore space effects because we analyzed intact chips, not powders.

The remaining broad continuum is probably due to oxidation of organic carbon by the indigenous oxygen and by small amounts of residual O_2 in the He flow of the instrument. Therefore, we can determine CO_2 contents from carbonate as shown in Figure 6. The organic carbon contents determined from Figure 6 are lower limits on the organic carbon contents because the TG-MS analysis cannot detect all organic carbon in the sample. Indeed, organic carbon and total carbon concentrations determined by the TG-MS were lower than those

determined by the combined analyses of pyrolysis and combustion (EMIA-Step) (*12*) (Data S6). We estimate that 74% of Ryugu organic carbon was released as the broad organic carbon continuum, as compared to 93% for Ivuna. Moreover, the release profiles of the broad organic carbon continuum are different for both samples. These results suggest that the organic components are not exactly the same for both Ryugu and Ivuna.

Many peaks are apparent in the H_2O release curves (Fig. 6). There are several sources of H_2O, e.g., the minor source is adsorbed H_2O from sulfates (at ~250 °C, Fig. 6), whereas the major source is H_2O from phyllosilicates (at ~600 °C, Fig. 6). The phyllosilicates consist of serpentine and saponite. Serpentine contains structural OH sites in the crystal structure, while saponite contains interlayer H_2O in addition to structural OH sites. The petrologic and mineralogic observations suggest that the sulfate contribution is insignificant for Ryugu, but significant for Ivuna. Indeed, the SO_2 and H_2O peak releases coincide in Ivuna (e.g., at 250 °C and 450 °C), but not Ryugu. Therefore, phyllosilicates are the dominant source of H_2O in the Ryugu sample.

From the results reported by (*46*) and the H_2O release curves displayed in Figure 6, dehydration of the interlayer H_2O of saponite is complete at 170 °C (the peak is at 90 °C) for Ryugu and at 350 °C (the peak is at 100 °C) for Ivuna. Dehydroxylation of structural OH in saponite and serpentine occurs at 300 – 800 °C for Ryugu and at 350–800 °C for Ivuna. The structural OH is dominant (6.54 H_2O wt.%) in the Ryugu sample, whereas the abundance of interlayer H_2O is small (0.30 H_2O wt.%). On the other hand, both types of H_2O are present at comparable levels in Ivuna (Data S6).

Inorganic/organic correlations for hydrogen and carbon contents

By the EMIA-Step analyses (*12*), the total carbon concentration and the organic carbon to total carbon fraction are 3.31 wt.% and 90 %, respectively, for our Ivuna sample (Fig. 7, Data S6), which are consistent with the results of (*47*). The total hydrogen and inorganic hydrogen to total hydrogen fraction are 1.59 wt.% and 89 % for Ivuna, respectively, which are also consistent with the results of (*47*). The total H_2O for Ivuna is 12.73 wt.%, and is distributed between interlayer and structural sites in the phyllosilicates: the interlayer H_2O is 6.58 wt.% and the structural-OH H_2O is 6.15 wt.%.

In contrast, Ryugu contains less H_2O than Ivuna. The total H_2O is 6.84 wt.% including 0.30 wt.% interlayer H_2O and 6.54 wt.% structural-OH H_2O (Data S6). Remarkably, the amount of structural-OH H_2O is similar between Ryugu and Ivuna. The total hydrogen is 0.94 wt.% for Ryugu, and the inorganic hydrogen (i.e., H_2O) comprises 81 % of the total hydrogen. The amount of organic carbon in Ryugu (3.08 wt.%) is essentially the same as in Ivuna (2.97 wt.%) (Fig. 7, Data S6), suggesting that inorganic/organic matter ratio is similar in the Ryugu and the Ivuna samples studied. This evidence would rule out the suggestion that Ryugu's low albedo is due to exceedingly high organic carbon contents (*48*). However, the total carbon is higher in Ryugu (4.63 wt.%) than in Ivuna due to the higher abundances of carbonates in the Ryugu samples.

Formation history of Ryugu

The CI-like elemental abundances of Ryugu suggest that all elements of the Solar System with 50 % condensation temperature higher than 500 K accreted into its parent body (probably closely related to the parent body(ies) of the CI chondrites) along with ice-forming elements (Fig. 2). The accreted material was likely mainly anhydrous dust and ice. The [53]Mn-

[53]Cr systematics of Ryugu dolomite, physical modeling of the thermal evolution of a water ice-bearing CI-like planetesimal (*14, 38*), and oxygen-isotope thermometry suggest that the Ryugu material accreted 2–4 million years after the birth of the Solar System. Approximately one to two million years later, or roughly 5 million years after the birth of the Solar System (Fig. 5), the Ryugu material experienced aqueous alteration resulting in precipitation of dolomite and magnetite from an aqueous solution at about 37 °C.

The aqueous alteration of the primary accreted Ryugu materials was very extensive. The saponite produced by this fluid-assisted alteration in the parent body of Ryugu must have contained significant interlayer water (~7 wt.%) in its crystal structure when it formed under saturated water activity, as observed in Ivuna (Data S6). The low abundance of interlayer water in the Ryugu samples (0.3 wt.%) indicates that it escaped to space, most likely after disruption of the parent body and formation of the asteroid Ryugu. The dehydration mechanism has yet to be definitively identified, but likely included some combination of impact heating, solar heating, space weathering, and long-term exposure of the asteroid surface to the ultra-high vacuum of space. A conservative estimate of the dehydration temperature would be 170 °C. However, if the dehydration temperature did reach to 170 °C, the interlayer water escaped completely from the Ryugu sample (Fig. 6). It is plausible that the Ryugu samples have not been heated above ~90 °C since their aqueous alteration because the small emission peak of interlayer water still remains at 90 °C (Fig. 6). The temperatures are not consistent with the thermal history of Ryugu estimated by (*6*). However, this is not surprising because the temperature estimated by (*6*) was not directly determined from the remote sensing data, but based mainly on laboratory heating experiments of carbonaceous chondrites. Therefore, the temperatures estimated in this study do not contradict the remote sensing data, and agrees with the surface temperature at the present orbit of Ryugu (*7*).

Some asteroids show comet-like activity, the origin of which is uncertain and could have involved several mechanisms (*49*). This activity can be subtle, as documented in the B-type asteroid Bennu visited by the OSIRIS-REx spacecraft, where plumes of dust particles and rocks were observed (*50*). These authors concluded that thermal fracturing, phyllosilicate dehydration, and meteoroid impact were the most plausible explanations for the ejection of solid particles from Bennu's surface. Our finding that saponite in Ryugu is partially dehydrated supports the view that volatile release associated with loss of loosely bound interlayer water in phyllosilicate can induce comet-like activity at the surface of low-perihelion carbonaceous asteroids. The mechanisms that we envision to lift dust and rocks from asteroidal surfaces may be (*i*) anisotropic release of water molecules from phyllosilicate-rich dust particles, imparting a net momentum to those particles, and (*ii*) buildup of vapor pressure in sealed pore space, leading eventually to their bursting and propelling dust particles away from the surface. Phyllosilicate dehydration could also play a role in the production of interplanetary dust particles and micrometeorites. The thermal release pattern of Ivuna (Fig. 6) shows that interlayer water is lost from saponite at a relatively low temperature of ~0 – 200 °C. The maximum surface temperatures of ~100 °C for Ryugu (*7*) and ~170 °C for Bennu (*51*) would therefore be sufficient for such devolatilization to take place. Such devolatilization is largely complete for surface particles on Ryugu. Current particle ejections from the asteroid surface were not observed by the Hayabusa2 spacecraft.

Implications for CI chondrites and cosmochemistry

The rare CI chondrites play a unique role in our understanding of the formation of the Solar System because among all meteorites, they are the ones whose elemental compositions

closely matches measurements of the solar photosphere composition (*52*) for all but the atmophile elements and lithium. CI chondrites experienced pervasive aqueous alteration, bearing witness to water-rock interactions in the early Solar System. All CI chondrites have been stored in meteorite collections for decades to centuries, and it is unknown the extent to which handling and exposure to atmospheric moisture modified their mineralogies and elemental compositions. Unlike CI chondrites that have fallen to the Earth, the Ryugu samples are nearly free of sulfates, ferrihydrite, and interlayer water. This could be due to either CI chondrites having originated on parent asteroids with higher water contents than Ryugu, or having been contaminated by terrestrial moisture during residence on Earth (*53, 54*). The lower abundance of anhydrous silicates and the small but clear shift in the $\Delta^{17}O$ measured in Ryugu relative to the Orgueil CI chondrite, and in the Orgueil measurements in this study (Fig. 4) compared to the previous work support the terrestrial contamination explanation. The slightly higher $\Delta^{17}O$ values of Orgueil in this study compared to earlier studies suggest that the O-isotope exchange in structural-OH water of CI chondrites could have happened even under room temperature conditions. Furthermore, the gas emission patterns of the TG-MS and EMIA-Step for Ryugu are clearly different from those measured in the Ivuna CI chondrite (Figs. 6 and 7). This suggests that the structures of the organic matter differ between Ryugu samples and the known CI chondrites and have been modified in the CI chondrites during residence on Earth. Indeed, some unique characteristics of organic matter have been observed in Ryugu samples (*55, 56*).

Our characterization of Ryugu samples suggests that they are chemically the most pristine Solar System materials analyzed to date in laboratories and that the materials observed in CI chondrites may be significantly changed/modified on the Earth from their primary states in space. CI chondrites may have been modified from their pre-atmospheric state by phyllosilicate hydration, organic matter transformation and contamination, adsorption/reaction of atmospheric components, and oxidation. These modifications might have changed the albedo, porosity, and density of the CI chondrites leading to the observed differences with the Ryugu samples (*5, 7, 10*). Because Ryugu material is the most chemically pristine member of the CI chondrite group known, it can provide a more reliable estimate of bulk Solar System elemental abundances.

References and Notes

1. H. Yurimoto *et al.*, Oxygen isotopic compositions of asteroidal materials returned from Itokawa by the Hayabusa mission. *Science* **333**, 1116-1119 (2011).
2. T. Nakamura *et al.*, Itokawa dust particles: A direct link between S-type asteroids and ordinary chondrites. *Science* **333**, 1113-1116 (2011).
3. S. Tachibana *et al.*, Hayabusa2: Scientific importance of samples returned from C-type near-Earth asteroid (162173) 1999 JU_3. *Geochem. J.* **48**, 571-587 (2014).
4. K. Kitazato *et al.*, The surface composition of asteroid 162173 Ryugu from Hayabusa2 near-infrared spectroscopy. *Science* **364**, 272-275 (2019).
5. S. Sugita *et al.*, The geomorphology, color, and thermal properties of Ryugu: Implications for parent-body processes. *Science* **364**, eaaw0422 (2019).
6. K. Kitazato *et al.*, Thermally altered subsurface material of asteroid (162173) Ryugu. *Nature Astronomy* **5**, 246-250 (2021).
7. T. Okada *et al.*, Highly porous nature of a primitive asteroid revealed by thermal imaging. *Nature* **579**, 518-522 (2020).
8. M. Grott *et al.*, Low thermal conductivity boulder with high porosity identified on C-type asteroid (162173) Ryugu. *Nature Astronomy* **3**, 971-976 (2019).

9. T. Morota *et al.*, Sample collection from asteroid (162173) Ryugu by Hayabusa2: Implications for surface evolution. *Science* **368**, 654-659 (2020).
10. T. Yada *et al.*, Preliminary analysis of the Hayabusa2 samples returned from C-type asteroid Ryugu. *Nature Astronomy* **6**, 214-220 (2021).
11. S. Tachibana *et al.*, Pebbles and sand on asteroid (162173) Ryugu: On-site observation and returned particles. *Science* **375**, 1011-1016 (2022).
12. Materials and methods are available as supplementary materials.
13. A. J. Brearley, in *Meteorites and the Early Solar System II,* D. S. Lauretta, H. Y. McSween, Eds. (University of Arizona Press, 2006), pp. 587-624.
14. T. Nakamura *et al.*, Formation and evolution of Cb-type asteroid Ryugu: direct evidence from returned samples. *Science* **in this issue**, (2022).
15. N. Dauphas, A. Pourmand, Thulium anomalies and rare earth element patterns in meteorites and Earth: Nebular fractionation and the nugget effect. *Geochim. Cosmochim. Acta* **163**, 234-261 (2015).
16. A.-C. Zhang *et al.*, Young asteroidal fluid activity revealed by absolute age from apatite in carbonaceous chondrite. *Nature Communications* **7**, 12844 (2016).
17. A. Morlok *et al.*, Brecciation and chemical heterogeneities of CI chondrites. *Geochim. Cosmochim. Acta* **70**, 5371-5394 (2006).
18. J. A. Barrat *et al.*, Geochemistry of CI chondrites: Major and trace elements, and Cu and Zn isotopes. *Geochim. Cosmochim. Acta* **83**, 79-92 (2012).
19. C. M. O'D. Alexander, R. Bowden, M. L. Fogel, K. T. Howard, Carbonate abundances and isotopic compositions in chondrites. *Meteorit. Planet. Sci.* **50**, 810-833 (2015).
20. J. T. Wasson, G. W. Kallemeyn, Compositions of chondrites. *Philosophical Transactions of the Royal Society of London. Series A, Mathematical and Physical Sciences* **325**, 535-544 (1988).
21. P. H. Warren: Stable-isotopic anomalies and the accretionary assemblage of the Earth and Mars: A subordinate role for carbonaceous chondrites. *Earth Planet Sci. Lett.* **311**, 93-100 (2011).
22. A. Trinquier *et al.*, Origin of nucleosynthetic isotope heterogeneity in the Solar protoplanetary disk. *Science* **324**, 374-376 (2009).
23. T. Kleine *et al.*, The non-carbonaceous–carbonaceous meteorite dichotomy. *Space Science Reviews* **216**, 55 (2020).
24. R. N. Clayton, T. K. Mayeda, Oxygen isotope studies of carbonaceous chondrites. *Geochim. Cosmochim. Acta* **63**, 2089-2104 (1999).
25. M. W. Rowe, R. N. Clayton, T. K. Mayeda, Oxygen isotopes in separated components of CI and CM meteorites. *Geochim. Cosmochim. Acta* **58**, 5341-5347 (1994).
26. M. Piralla *et al.*, Primordial water and dust of the Solar System: Insights from in situ oxygen measurements of CI chondrites. *Geochim. Cosmochim. Acta* **269**, 451-464 (2020).
27. Y.-f. Zheng, Calculation of oxygen isotope fractionation in metal oxides. *Geochim. Cosmochim. Acta* **55**, 2299-2307 (1991).
28. Y.-F. Zheng, Oxygen isotope fractionation in carbonate and sulfate minerals. *Geochem. J.* **33**, 109-126 (1999).
29. Y.-F. Zheng, On the theoretical calculations of oxygen isotope fractionation factors for carbonate-water systems. *Geochem. J.* **45**, 341-354 (2011).
30. Y.-F. Zheng, Calculation of oxygen isotope fractionation in hydroxyl-bearing silicates. *Earth Planet. Sci. Lett.* **120**, 247-263 (1993).

31. W. Guo, Carbonate clumped isotope thermometry: Applications to carbonaceous chondrites and effects of kinetic isotope fractionation. *Dissertation (Ph.D.), California Institute of Technology*, 261 pp (2009).

32. L. A. Leshin, A. E. Rubin, K. D. McKeegan, The oxygen isotopic composition of olivine and pyroxene from CI chondrites. *Geochim. Cosmochim. Acta* **61**, 835-845 (1997).

33. E. S. Bullock, M. Gounelle, D. S. Lauretta, M. M. Grady, S. S. Russell, Mineralogy and texture of Fe-Ni sulfides in CI1 chondrites: Clues to the extent of aqueous alteration on the CI1 parent body. *Geochim. Cosmochim. Acta* **69**, 2687-2700 (2005).

34. R. Visser, T. John, M. Menneken, M. Patzek, A. Bischoff, Temperature constraints by Raman spectroscopy of organic matter in volatile-rich clasts and carbonaceous chondrites. *Geochim. Cosmochim. Acta* **241**, 38-55 (2018).

35. E. L. Berger, L. P. Keller, D. S. Lauretta, An experimental study of the formation of cubanite ($CuFe_2S_3$) in primitive meteorites. *Meteorit. Planet. Sci.* **50**, 1-14 (2015).

36. E. R. Dufresne, E. Anders, On the chemical evolution of the carbonaceous chondrites. *Geochim. Cosmochim. Acta* **26**, 1085-1114 (1962).

37. M. E. Zolensky, W. L. Bourcier, J. L. Gooding, Aqueous alteration on the hydrous asteroids: Results of EQ3/6 computer simulations. *Icarus* **78**, 411-425 (1989).

38. W. Fujiya, N. Sugiura, Y. Sano, H. Hiyagon, Mn–Cr ages of dolomites in CI chondrites and the Tagish Lake ungrouped carbonaceous chondrite. *Earth Planet. Sci. Lett.* **362**, 130-142 (2013).

39. R. Visser, T. John, M. J. Whitehouse, M. Patzek, A. Bischoff, A short-lived [26]Al induced hydrothermal alteration event in the outer solar system: Constraints from Mn/Cr ages of carbonates. *Earth Planet. Sci. Lett.* **547**, 116440 (2020).

40. D. P. Glavin, A. Kubny, E. Jagoutz, G. W. Lugmair, Mn-Cr isotope systematics of the D'Orbigny angrite. *Meteorit. Planet. Sci.* **39**, 693-700 (2004).

41. G. A. Brennecka, M. Wadhwa, Uranium isotope compositions of the basaltic angrite meteorites and the chronological implications for the early Solar System. *Proceedings of the National Academy of Sciences of the United States of America* **109**, 9299-9303 (2012).

42. J. N. Connelly *et al.*, The absolute chronology and thermal processing of solids in the solar protoplanetary disk. *Science* **338**, 651-655 (2012).

43. F. L. H. Tissot, N. Dauphas, T. L. Grove, Distinct [238]U/[235]U ratios and REE patterns in plutonic and volcanic angrites: Geochronologic implications and evidence for U isotope fractionation during magmatic processes. *Geochim. Cosmochim. Acta* **213**, 593-617 (2017).

44. A. Trinquier, J. L. Birck, C. J. Allègre, C. Göpel, D. Ulfbeck, [53]Mn–[53]Cr systematics of the early Solar System revisited. *Geochim. Cosmochim. Acta* **72**, 5146-5163 (2008).

45. L. E. Nyquist, T. Kleine, C. Y. Shih, Y. D. Reese, The distribution of short-lived radioisotopes in the early solar system and the chronology of asteroid accretion, differentiation, and secondary mineralization. *Geochim. Cosmochim. Acta* **73**, 5115-5136 (2009).

46. A. J. King, J. R. Solomon, P. F. Schofield, S. S. Russell, Characterising the CI and CI-like carbonaceous chondrites using thermogravimetric analysis and infrared spectroscopy. *Earth, Planets and Space* **67**, 198 (2015).

47. C. M. O'D. Alexander *et al.*, The provenances of asteroids, and their contributions to the volatile inventories of the terrestrial planets. *Science* **337**, 721-723 (2012).

48. C. Potiszil, R. Tanaka, K. Kobayashi, T. Kunihiro, E. Nakamura, The albedo of Ryugu: Evidence for a high organic abundance, as inferred from the Hayabusa2 touchdown maneuver. *Astrobiology* **20**, 916-921 (2020).

49. D. Jewitt, H. Hsieh, J. Agarwal, in *Asteroids IV,* P. Michel, F. E. DeMeo, W. F. Bottke, Eds. (University of Arizona Press, Tucson, 2015), pp. 221-241.

50. D. S. Lauretta *et al.*, Episodes of particle ejection from the surface of the active asteroid (101955) Bennu. *Science* **366**, eaay3544 (2019).

51. D. N. DellaGiustina *et al.*, Properties of rubble-pile asteroid (101955) Bennu from OSIRIS-REx imaging and thermal analysis. *Nature Astronomy* **3**, 341-351 (2019).

52. K. Lodders, Relative atomic solar system abundances, mass fractions, and atomic masses of the elements and their isotopes, composition of the solar photosphere, and compositions of the major chondritic meteorite groups. *Space Science Reviews* **217**, 44 (2021).

53. M. Gounelle, M. E. Zolensky, The Orgueil meteorite: 150 years of history. *Meteorit. Planet. Sci.* **49**, 1769-1794 (2014).

54. L. Baker, I. A. Franchi, I. P. Wright, C. T. Pillinger, The oxygen isotopic composition of water from Tagish Lake: Its relationship to low-temperature phases and to other carbonaceous chondrites. *Meteorit. Planet. Sci.* **37**, 977-985 (2002).

55. H. Naraoka *et al.*, Organic compounds from Ryugu – Prebiotic molecules in a C-type asteroid. *Science* **this issue**,   (2022).

56. H. Yabuta *et al.*, Macromolecular organic materials recording aqueous activity on parent body of the asteroid Ryugu. *Science* **this issue**,   (2022).

57. A. Bischoff *et al.*, The old, unique C1 chondrite Flensburg – Insight into the first processes of aqueous alteration, brecciation, and the diversity of water-bearing parent bodies and lithologies. *Geochim. Cosmochim. Acta* **293**, 142-186 (2021).

58. J. Alfing, M. Patzek, A. Bischoff, Modal abundances of coarse-grained (>5 μm) components within CI-chondrites and their individual clasts – Mixing of various lithologies on the CI parent body(ies). *Geochemistry* **79**, 125532 (2019).

59. N. Dauphas, E. A. Schauble, Mass Fractionation Laws, Mass-Independent Effects, and Isotopic Anomalies. *Annu. Rev. Earth Planet. Sci.* **44**, 709-783 (2016).

60. C. Burkhardt *et al.*, In search of the Earth-forming reservoir: Mineralogical, chemical, and isotopic characterizations of the ungrouped achondrite NWA 5363/NWA 5400 and selected chondrites. *Meteorit. Planet. Sci.* **52**, 807-826 (2017).

61. J. Sherman, The theoretical derivation of fluorescent X-ray intensities from mixtures. *Spectrochimica Acta* **7**, 283-306 (1955).

62. T. Shiraiwa, N. Fujino, Theoretical calculation of fluorescent X-ray intensities in fluorescent X-ray spectrochemical analysis. *Jpn. J. Appl. Phys.* **5**, 886-899 (1966).

63. S. Komatani, S. Ohzawa, Development of the XGT-5000 X-ray Analytical Microscope. *Readout English Edition (HORIBA Technical Reports)* **9**, 80-83 (2005).

64. Y. Abe, R. Shikaku, I. Nakai, Ancient glassware travelled the Silk Road: Nondestructive X-ray fluorescence analysis of tiny glass fragments believed to be sampled from glassware excavated from Niizawa Senzuka Tumulus No. 126, Japan. *Journal of Archaeological Science: Reports* **17**, 212-219 (2018).

65. T. Yokoyama, Y. Nagai, Y. Hinohara, T. Mori, Investigating the influence of non-spectral matrix effects in the determination of twenty-two trace elements in rock samples by ICP-QMS. *Geostandard. Geoanalytic. Res.* **41**, 221-242 (2017).

66. S. Kagami, T. Yokoyama, Simultaneous determination of insoluble fluoride-forming and high field-strength element abundances in rock samples by ICP-QMS through isotope dilution-internal standardisation. *Geostandards and Geoanalytical Research* **45**, 679-699 (2021).

67. Yokoyama et al. Multi-isotopic analyses of bulk Ryugu samples returned by the Hayabusa2 mission. *53rd Lunar and Planetary Science Conference*, The Woodlands, TX. Abstract #1273 (2022).

68. I. Leya, M. Schönbächler, U. Wiechert, U. Krähenbühl, A. N. Halliday, High precision titanium isotope measurements on geological samples by high resolution MC-ICPMS. *Int. J. Mass Spectrom.* **262**, 247-255 (2007).

69. G. D. Flesch, J. Capellen, H. J. Svec, in *Advanced Mass Spectrometry,* W. L. Mead, Ed. (Leiden and Son, London, 1966), vol. 3, pp. 571-581.

70. W. R. Shields, T. J. Murphy, E. J. Catanzaro, E. L. Garner, Absolute isotopic abundance ratios and the atomic weight of a reference sample of chromium. *Journal of research of the National Bureau of Standards. Section A, Physics and chemistry* **70**, 193 (1966).

71. J. Zhang, N. Dauphas, A. M. Davis, A. A. Pourmand, A new method for MC-ICPMS measurement of titanium isotope composition: Identification of correlated isotope anomalies in meteorites. *Journal of Analytical Atomic Spectrometry* **26**, 2197-2205 (2011).

72. Z. D. Sharp, A laser-based microanalytical technique for in situ determination of oxygen isotope ratios of silicates and oxides. *Geochim. Cosmochim. Acta* **54**, 1353-1357 (1990).

73. A. Pack, Isotopic traces of atmospheric O_2 in rocks, minerals, and melts. *Rev. Mineral. Geochem.* **86**, 217-240 (2021).

74. E. D. Young, A. Galy, H. Nagahara, Kinetic and equilibrium mass-dependent isotope fractionation laws in nature and their geochemical and cosmochemical significance. *Geochim. Cosmochim. Acta* **66**, 1095-1104 (2002).

75. E. D. Young, L. Y. Yeung, I. E. Kohl, On the $\Delta^{17}O$ Budget of Atmospheric O_2. *Geochim. Cosmochim. Acta* **135**, 102-125 (2014).

76. N. Kawasaki, S. B. Simon, L. Grossman, N. Sakamoto, H. Yurimoto, Crystal growth and disequilibrium distribution of oxygen isotopes in an igneous Ca-Al-rich inclusion from the Allende carbonaceous chondrite. *Geochim. Cosmochim. Acta* **221**, 318-341 (2018).

77. M. G. Śliwiński *et al.*, Secondary ion mass spectrometry bias on isotope ratios in dolomite–ankerite, Part I: $\delta^{18}O$ Matrix Effects. *Geostandards and Geoanalytical Research* **40**, 157-172 (2016).

78. K. Nagashima *et al.*, Investigation of instrumental fractionation in SIMS analyses of magnesium, silicon, and oxygen isotopes in silicates and oxides. *51th LPSC*, abstract#1719 (2020).

79. J. M. Huberty *et al.*, Crystal orientation effects in $\delta^{18}O$ for magnetite and hematite by SIMS. *Chemical Geology* **276**, 269-283 (2010).

80. K. P. Jochum *et al.*, Nano-powdered calcium carbonate reference materials: Significant progress for microanalysis? *Geostandards and Geoanalytical Research* **43**, 595-609 (2019).

81. R. C. J. Steele, V. S. Heber, K. D. McKeegan, Matrix effects on the relative sensitivity factors for manganese and chromium during ion microprobe analysis of carbonate: Implications for early Solar System chronology. *Geochim. Cosmochim. Acta* **201**, 245-259 (2017).

82. K. Ichimura and N. Sugiura, Preparation of synthetic dolomite for determination of Mn/Cr relative sensitivity. *46th LPSC*, abstract#1795 (2015).

83. P. H. Donohue, G. R. Huss, and K. Nagashima, New synthetic carbonates for investigation of manganese-chromium chronology by secondary ion mass spectrometry. *50th LPSC*, abstract#1959 (2019).

84. K. A.McCain, M.-C.Liu, and K. D. McKeegan, Calibration of matrix-dependent biases in isotope and trace element analyses of carbonate minerals. *J. Vac. Sci. Technol.* **B 38**, 044005 (2020).

85. P. Vermeesch, IsoplotR: A free and open toolbox for geochronology. *Geoscience Frontiers* **9**, 1479-1493 (2018).

86. A. Trinquier, J. L.Birck, C. J. Allegre, Widespread Cr-54 heterogeneity in the inner solar system. *Astrophys. J.* **655**, 1179-1185 (2007).

87. C. M. O'D. Alexander, M. Fogel, H. Yabuta, G. D. Cody, The origin and evolution of chondrites recorded in the elemental and isotopic compositions of their macromolecular organic matter. *Geochim. Cosmochim. Acta* **71**, 4380-4403 (2007).

Supplementary Materials

Materials and Methods

Supplementary Text

Figs. S1 to S2

Data S1 to S8

References (*61–87*)
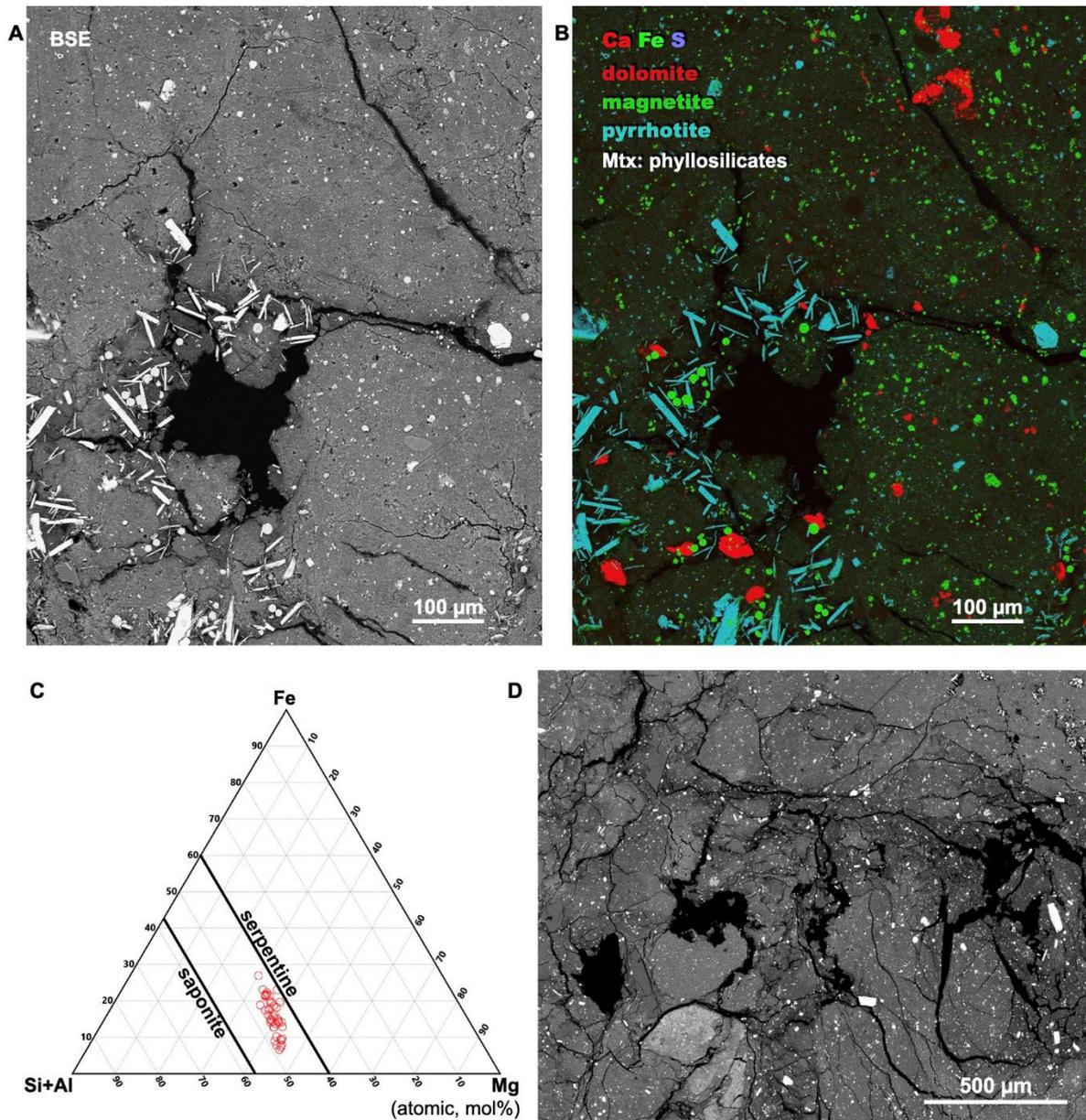
Fig. 1. Petrography of Ryugu sample. (**A**) Backscattered electron (BSE) image and (**B**) combined characteristic X-ray elemental map in Ca Kα (red), Fe Kα (green), S Kα (blue) of A0058-C1001 (*12*), showing carbonate (dolomite), sulfide (pyrrhotite) and iron-oxide (magnetite) minerals precipitated in veinlets. The sulfide texture is similar to that in the C1 chondrite Flensburg *(57)*. (**C**) Bulk chemical composition of matrix in A0058-C1001. (**D**) BSE image of C0002-C1001, showing brecciated matrix. Note texture similarities with CI chondrites *(58)*.
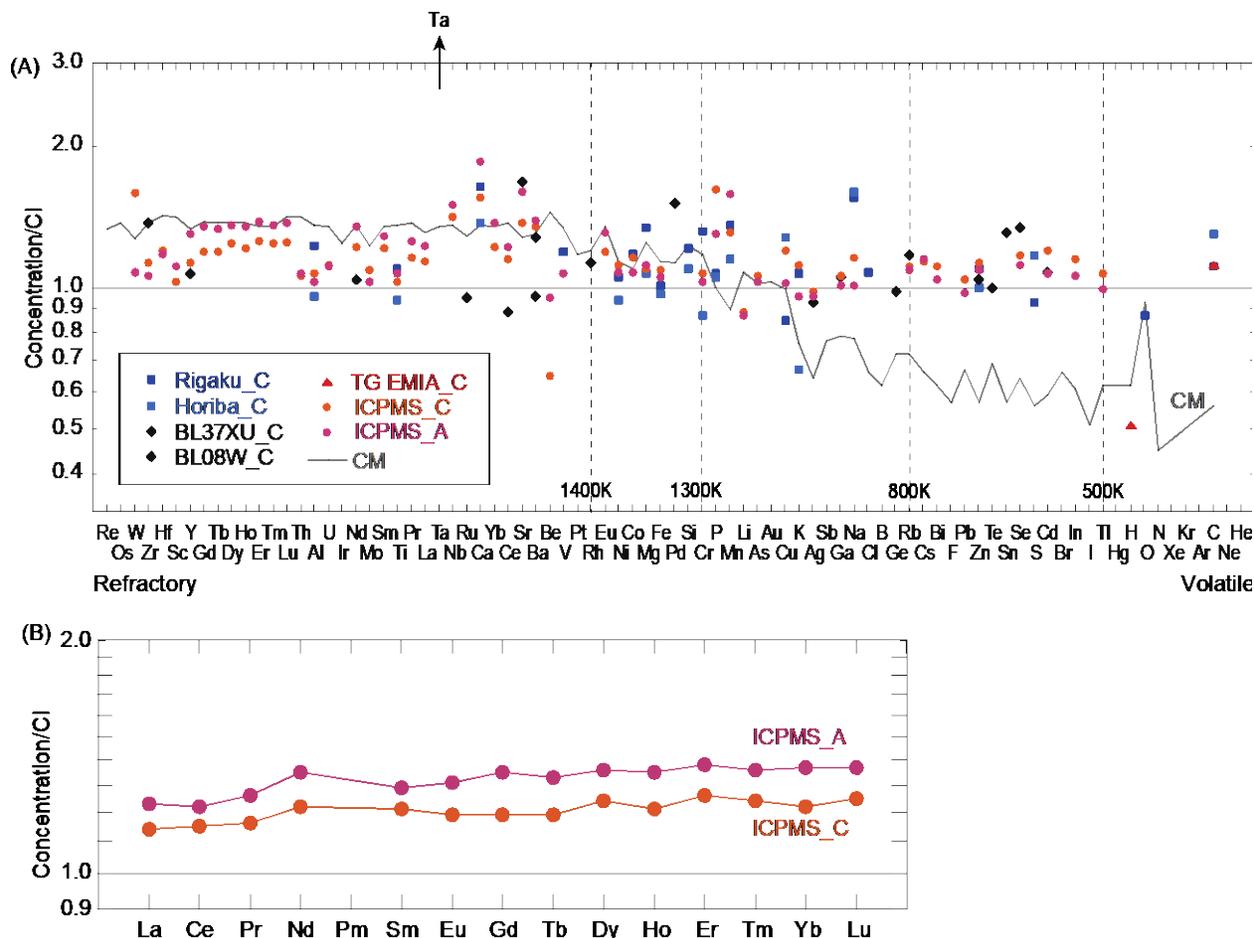
Fig. 2. Elemental abundances of Ryugu relative to CI chondrite (*52*) **as a function of 50 % condensation temperature** (*52*) **(A) and REE pattern (B).** There are no systematic depletions of the elemental abundances with elemental volatilities. The high abundances of tantalum (upward arrow) reflect contaminants from the Ta projectiles used in the sampling apparatus of Hayabusa2 that impacted the Ryugu surfaces (*12*). A and C are samples from Touchdown sites #1 and #2, respectively. Rigaku_C: XRF analysis using laboratory X-rays at Rigaku company, Horiba_C: XRF analysis using laboratory X-rays at Horiba company, BL37XU_C and BL08W_C: XRF analysis using synchrotron radiation at SPring-8, TG EMIA_C: combination of thermogravimetric analysis coupled with mass spectrometry and pyrolysis/combustion analysis at Rigaku and Horiba, ICP MS_C and ICP MS_A: ICP-MS at Tokyo Tech., CM: representative value of CM chondrites (*52*). Data are shown in Data S2 (*12*).
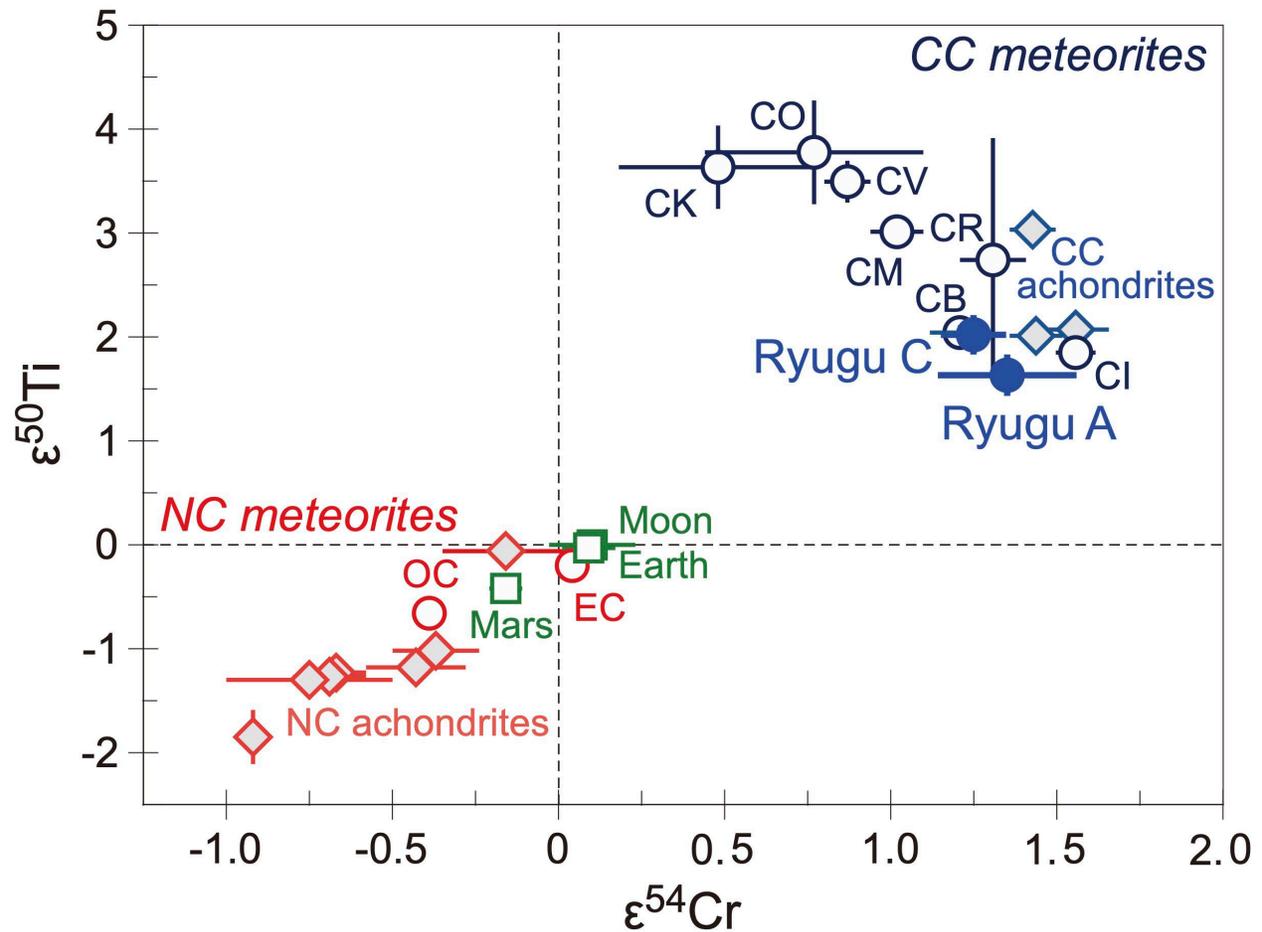
Fig. 3. Ti-Cr isotope systematics of Ryugu. The Ryugu values plot near the CB and CI chondrite values in the CC meteorites region. CC: Carbonaceous, NC: Non-carbonaceous. CI, CM, CO, CV, CK, CR, CB: groups of carbonaceous chondrite class, OC: ordinary chondrite class, EC: enstatite chondrite class. The CC achondrites and NC achondrites are differentiated stony meteorites that have Ti and Cr isotopic compositions similar to CC and NC meteorites, respectively. Data except Ryugu from (*22, 59, 60*). Data of Ryugu are shown in Data S3 (*12*).
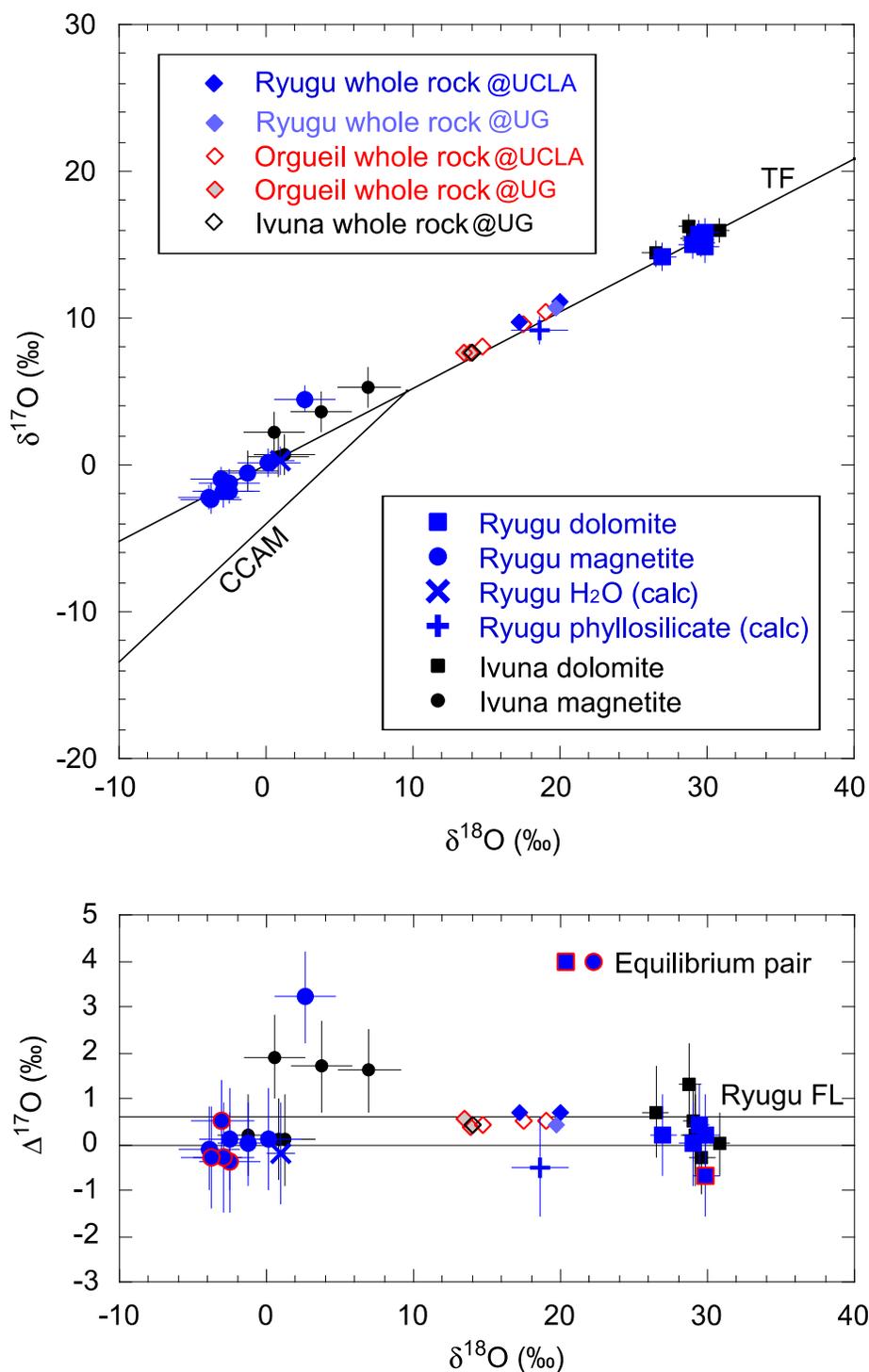
Fig. 4. Oxygen isotopic compositions of Ryugu, Ivuna, and Orgueil. Oxygen isotopic compositions of H_2O and phyllosilicate of Ryugu are calculated from equilibrium pair between dolomite and magnetite (symbols rimmed by read line) shown in Figure S1 (*12*). The oxygen isotopic characteristics of Ryugu resemble those of the CI chondrites. TF: terrestrial mass fractionation line, CCAM: carbonaceous chondrite anhydrous mineral line, Ryugu FL: mass fractionation line of Ryugu. Data are shown in Data S4 (*12*).
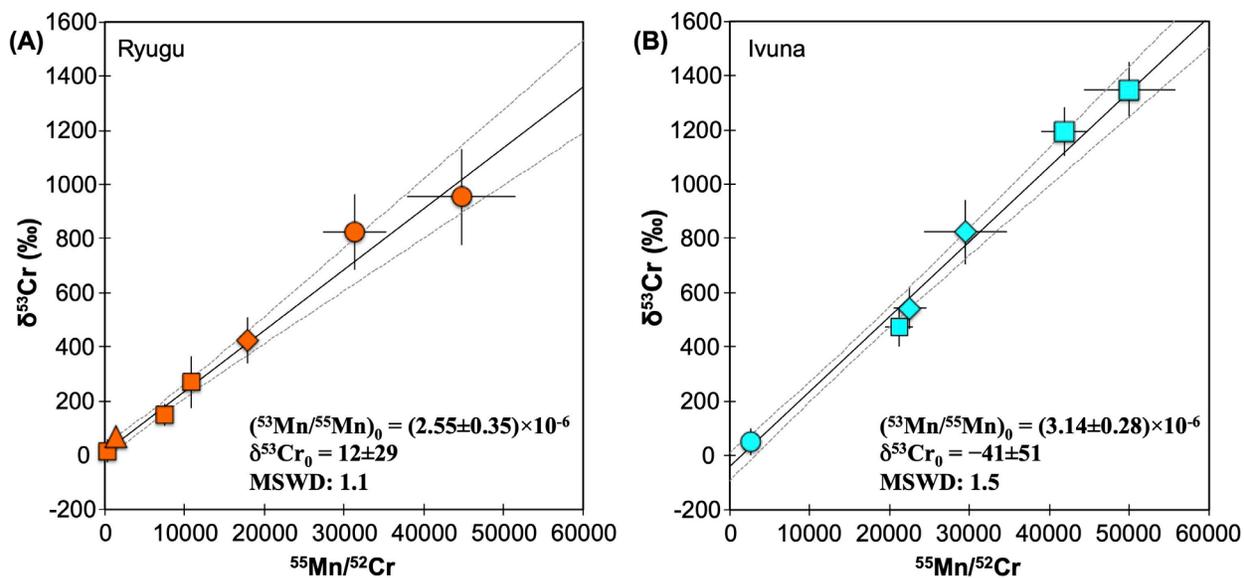
Fig. 5. ^{53}Mn-^{53}Cr systematics for dolomite from Ryugu (A) and Ivuna (B). The same symbol corresponds to measurements in the same crystal. The isochron for Ryugu suggests that dolomite precipitation occurred at 5.2 (+0.8/-0.7) million years after the birth of the Solar System. Data are shown in Data S5 (*12*).
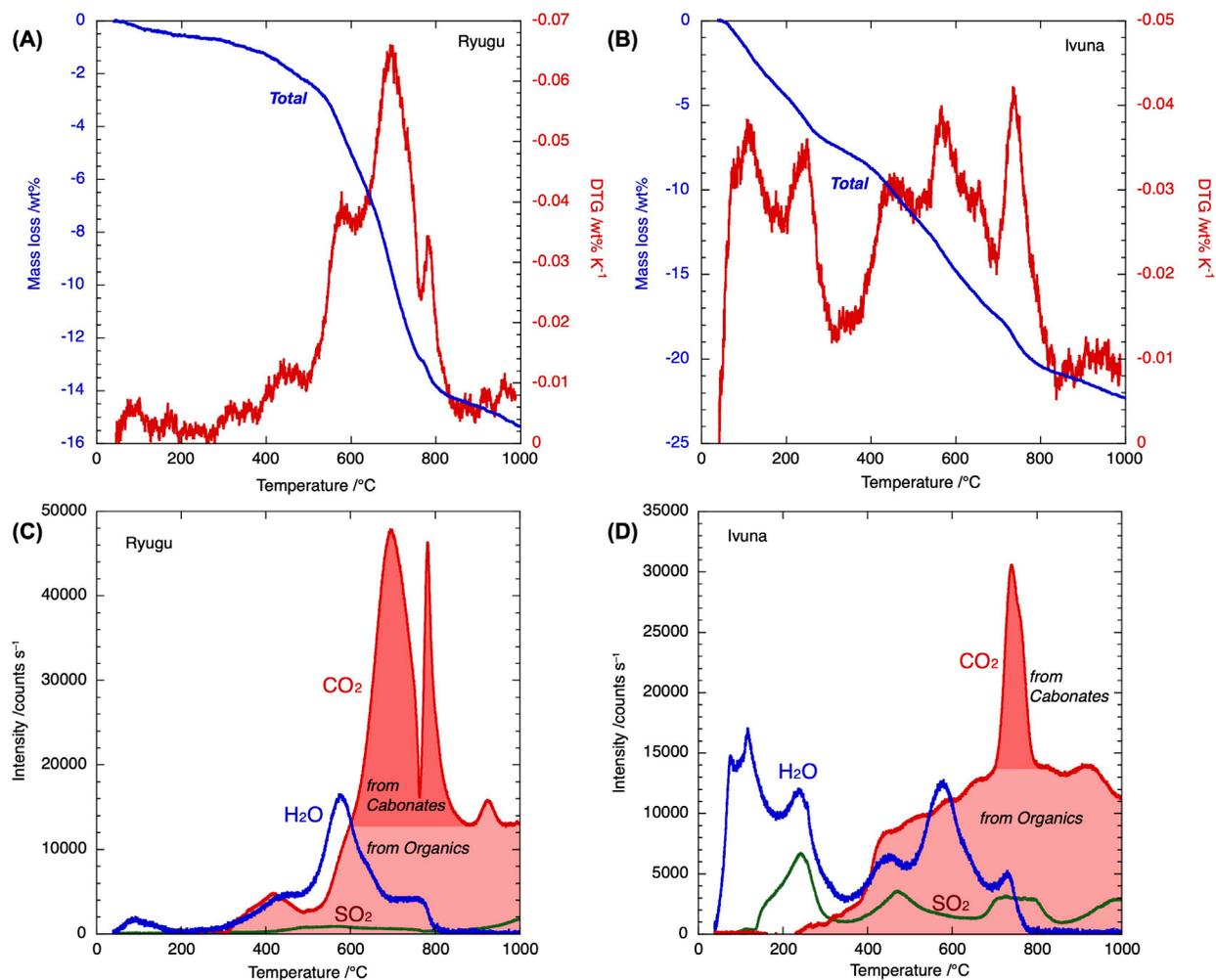
Fig. 6. Thermogravimetric analysis coupled with mass spectrometry (TG-MS) for Ryugu and Ivuna. Mass loss (blue) and DTG (red) curves for Ryugu (**A**) and Ivuna (**B**). Mass intensity curves generated from Ryugu (**C**) and Ivuna (**D**). H_2O: m/z =18, CO_2: m/z =44, SO_2: m/z =64. Contributions from carbonates and organics for CO_2 curve are shown by the different colors. Data are shown in Data S7 (*12*).
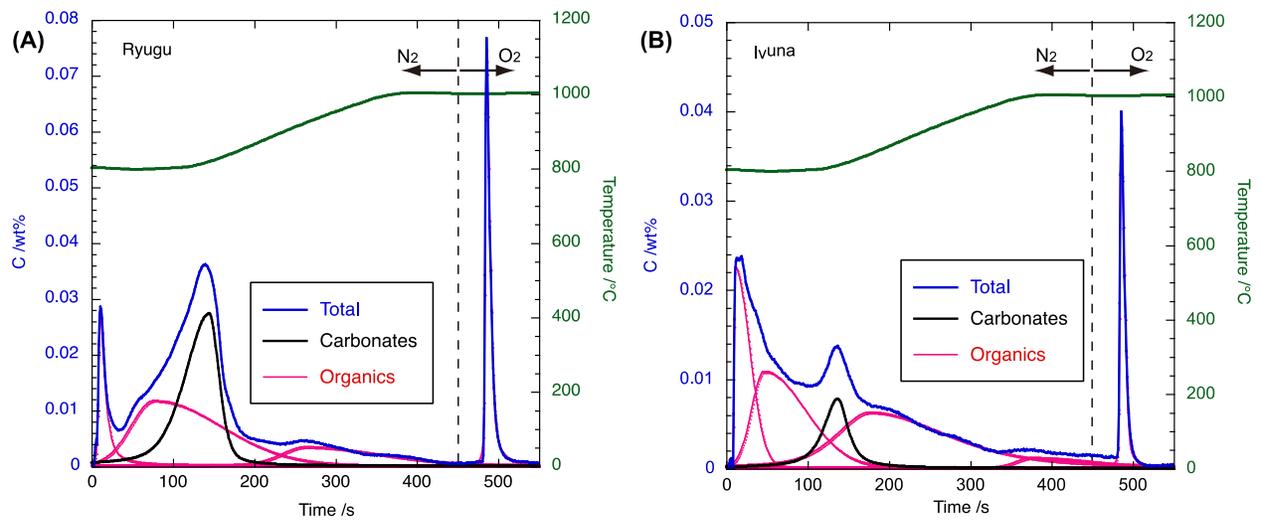
Fig. 7. CO₂ curve generated from Ryugu (A) and Ivuna (B) by combination of pyrolysis and combustion analyses with step heating (EMIA-Step). Data are shown in Data S8 (*12*).